ISSN 0016-7029, Geochemistry International, 2012, Vol. 50, No. 9, pp. 777–790. © Pleiades Publishing, Ltd., 2012.
Original Russian Text © M. Khanehbad, R. Moussavi-Harami, A. Mahboubi, M. Nadjafi, 2012, published in Geokhimiya, 2012, Vol. 50, No. 9, pp. 867–880.

Geochemistry of Carboniferous Shales of the Sardar Formation, East Central Iran: Implication for Provenance, Paleoclimate and Paleo-oxygenation Conditions at a Passive Continental Margin

M. Khanehbad, R. Moussavi-Harami, A. Mahboubi and M. Nadjafi

Department of Geology, Faculty of Sciences, Ferdowsi University of Mashhad, Mashhad, Iran

e-mail: mkhanehbad@ferdowsi.um.ac.ir

Received November 20, 2010; in final form October 11, 2011

Abstract—The Sardar Formation (Carboniferous) has a lithological variation that is characterized by sandstone, shale and limestone members. Shales of the Sardar Formation from the east central Iran have been analyzed for major elements and a number of trace elements. The shales of Sardar Formation are rich in quartz minerals and clay minerals of the bulk minerals. Clay minerals of shales are composed of illite, kaolinite and slightly montmorillonite. SiO_2 versus K_2O/Na_2O diagram shows these shales plotted in the passive continental margin or cratonic field. Geochemical data suggest high acidic source rocks similar to granite and intermediate igneous rocks. CIA and ICV suggest semi-humid climatic conditions during depositions and indicate high chemical weathering in the source area. The geochemical parameters such as V/Cr, Ni/Co and Cu/Zn ratios indicate that these shales were deposited in oxic environment.

Keywords: provenance,paleoclimate, passive margin, Sardar Formation, Iran

DOI: 10.1134/S0016702912090029

1. INTRODUCTION

Shale is the most abundant type of sedimentary rocks exposed at the earth surface [1]. It shows the average crustal composition of the provenance very much better than any other detrital sedimentary rocks [2]. The geochemistry of shales is mostly used for provenance interpretations compared to the petrography approach used for sandstones [3–6]. The bulk geochemistry of mudrocks shows the real original signatures for provenance and reflects paleoweathering and diagenetic history. Trace element such as La, Y, Sc, Cr, Th, Zr, Hf, Nb, and particularly Ti are the best suites for provenance and tectonic setting studies due to their relatively low mobility during sedimentary processes [7]. Major oxides, such as TiO_2 and Al_2O_3, and trace elemental analysis are commonly used for provenance interpretations. For example, contributions of trace elements, zirconium, lanthanum, barium and vanadium, in mudrocks provides information about conditions of source rocks in combination with different binary and ternary plots of other elements [8–19].

The purpose of this paper is to describe the major and trace element geochemistry of shales from the Sardar Formation (Carboniferous) in the east central Iran and interpret provenance, paleotectonic and paleoweathering. This study allows for a better understanding of paleogeographic reconstruction of Carboniferous period in a remote area of Central Iran.

[1] The article is published in the original

2. GEOLOGY AND STRATIGRAPHY

Structurally, the study areas are located in the Tabas Block, east central Iran. The Paleozoic succession of east central Iran was deposited in north-south trending Tabas Block which was bounded by the Nayband right-lateral strike slip fault in the east and the Kalmard-Kuhbanan right-lateral strike slip fault in the west [20]. Central Iran, along with the Alborz Mountains of northern Iran, is located between the Neotethys and Paleotethys suture zone of Iran and are a part of the Cimmerian Continent [21], which was separated from the Gondwana super-continent during the Permian time [22–25], The Tabas Block is a part of the Cimmerian continent covers an area of approximately 50.000 square kilometers [26]. Based on regional facies and sequence stratigraphic analyses of the Paleozoic deposits of Iran [25], the Tabas Block considered as a failed rift basin, which is related to the Paleotethys margin during Devonian to Late Triassic time. This block was separated, along with the rest of the Cimmerian Plate, from northern Gondwana during the Permian.

The Sardar Formation (Carboniferous) crops out along the bounding faults of the Tabas Block and is distinguished by its characteristic siliciclastic facies in the field (Figs. 1, 2). The Sardar Formation unconformably overlies the Member 2 of the Shishtu Formation (Early Carboniferous), which is about 220 meters thick and consists mainly of gray, thin to intermediate bedded limestone and is unconformably overlain by the Permian Jamal Formation, which is over 500 meters thick

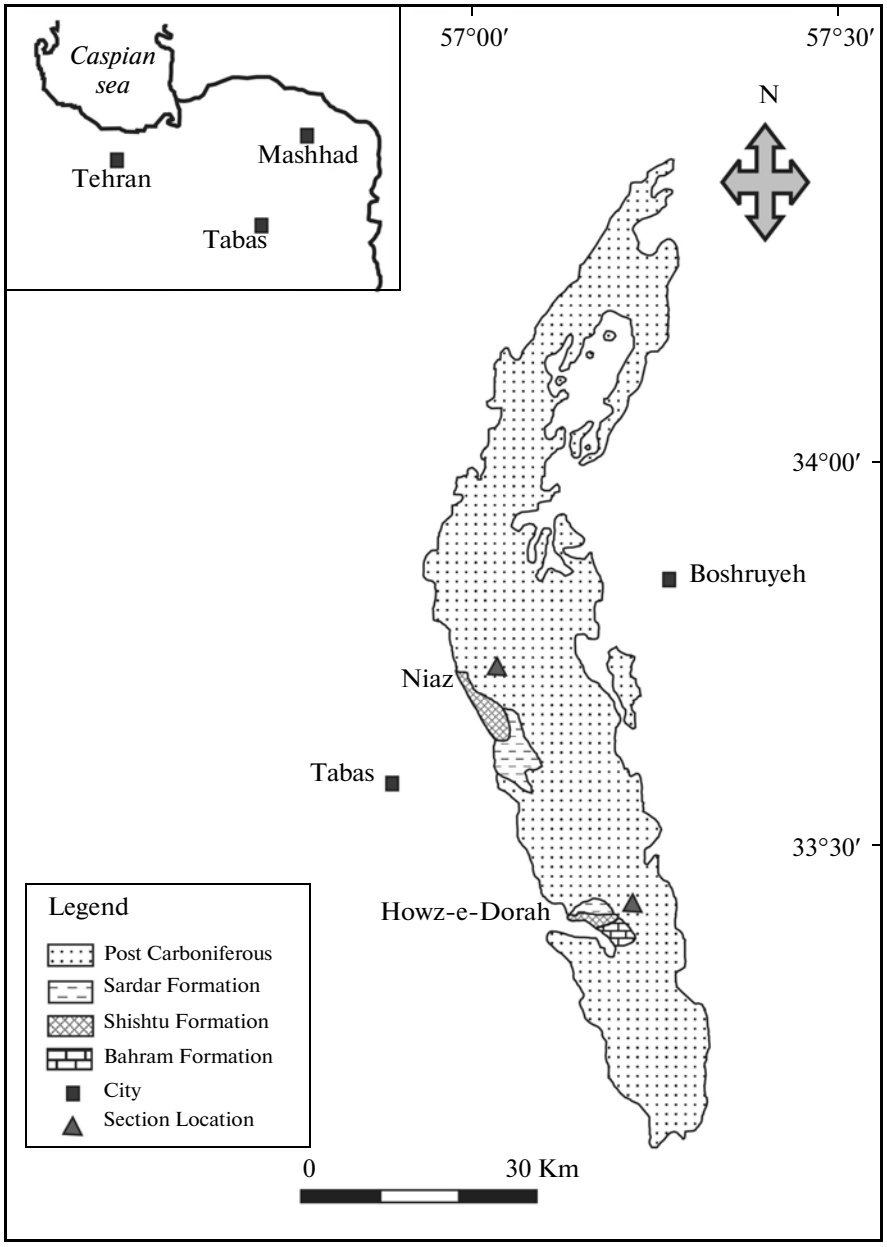

Fig. 1. Simplified geologic map of the study area.

and consists of thick bedded to massive limestone and dolomite. Figure 1 shows the lower part of the Shishtu Formation (Member 1), Upper Devonian in age includes mostly well-bedded grey limestone intercalated with siltstone and claystone that overlies the fossiliferous limestone of Bahram Formation (Middle to Late Devonian in age). The Sardar Formation occurs in two disconnected large outcrops (Fig. 1), one at the west foot of Kuh-e-Shotori across the Sardar valley (Niaz section with 656 m thickness), and the other at the south-foot of Kuh-e-Jamal (Howz-e-Dorah section with 584 m thickness). The type section (Niaz section) is not an ideal section, because the lowermost part of the formation and its contact with older rocks is not exposed. However, Howz-e-Dorah section is introduced as reference section in this study, in order to illustrate the contact relations with the underlying rocks. The sedimentary succession of the Sardar Formation consists of alternating sandstones, shales and limestones.

3. METHODS

Two stratigraphic sections (Niaz and Howz-e-Dorah localities) were measured, described and sampled in the field (Fig. 3). A total of 285 samples of sandstone, limestone and shale were collected in the field. 21 shale samples were used for analysis of major and

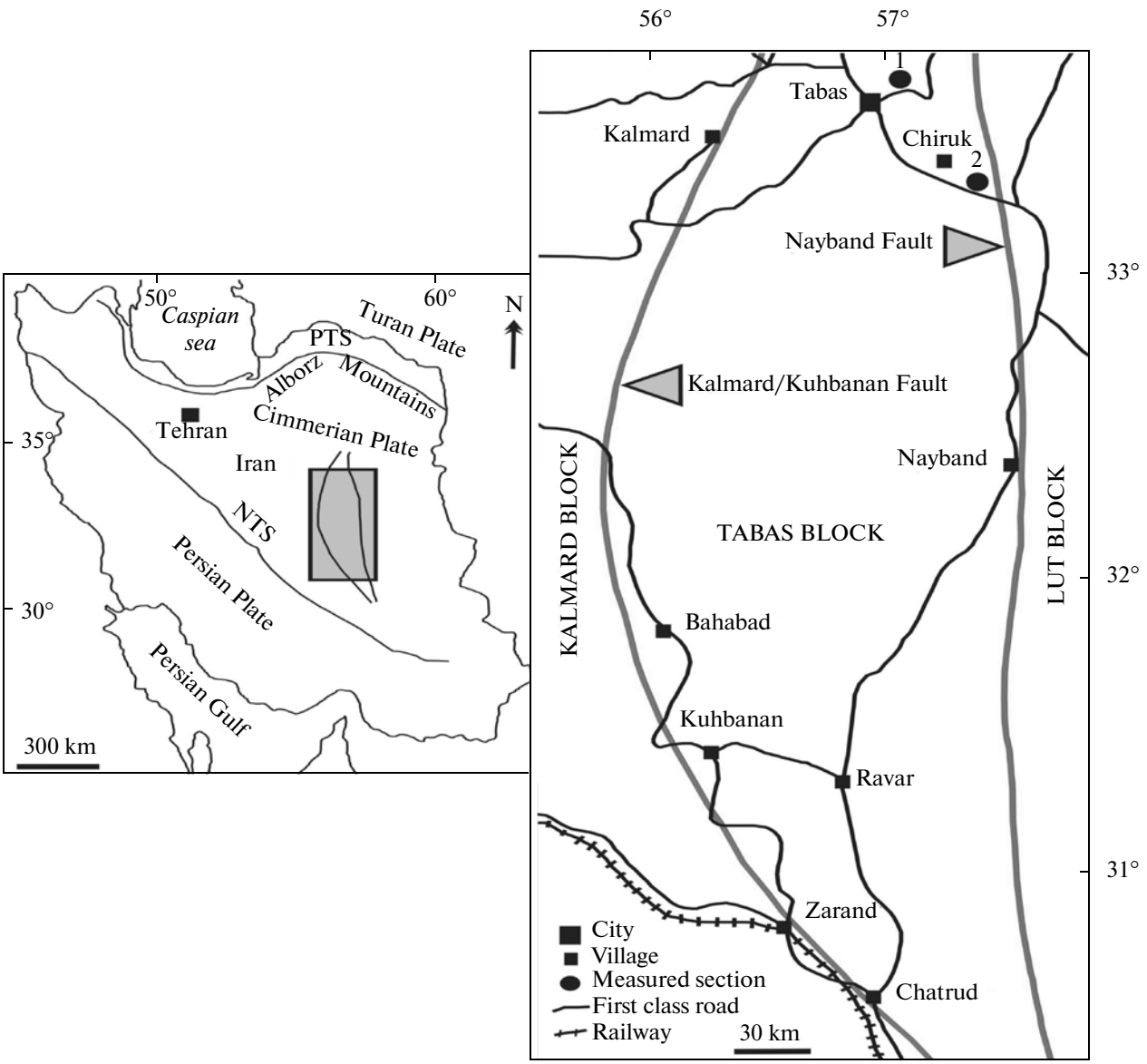

Fig. 2. Location map of the Tabas Block (between the Kalmard-Kuhbanan Fault in the west and the Nayband Fault in the east) in east central Iran (1: Niaz section, 2: Howz-e-Dorah section). The area between the Paleotethys suture (PTS) and Neotethys suture (NTS) on the index map comprises the Cimmerian plates of central and northern Iran (modified after [26]).

trace elements and mineralogy. The major and trace element concentrations were determined by X-ray fluorescence spectrometer (XRF) at Spectrum Kansaran Binaloud (Mine Material Research Co.), Mashhad, Iran (Philips PW 1480 X-ray spectrometer). Same samples of shales analyzed with X- ray diffraction (XRD) that the information of the machines is Philips X'pert diffractometer system.

4. RESULT AND DISCUSSION

4.1. Clay Mineralogy

The X-ray diffraction studies on the bulk shale show that all the studied samples are mainly composed of quartz associated with clay minerals, K-feldspar and plagioclase. The principal clay minerals are kaolinite and illite (Fig. 4). Feldspar, gypsum and calcite occur only in minor amounts. The XRD patterns of whole-rock samples show that shales of the Sardar Formation are rich in quartz associated with clay mineral such as kaolinite, illite and slightly montmorillonite. For shales, clay mineralogy has been the mineralogical procedure most often applied to reconstruct provenance.

4.2. Source Rocks for Shales of Sardar Formation

Shales are best favor for provenance studies of siliciclastic sediments due to their commonly homogeneity

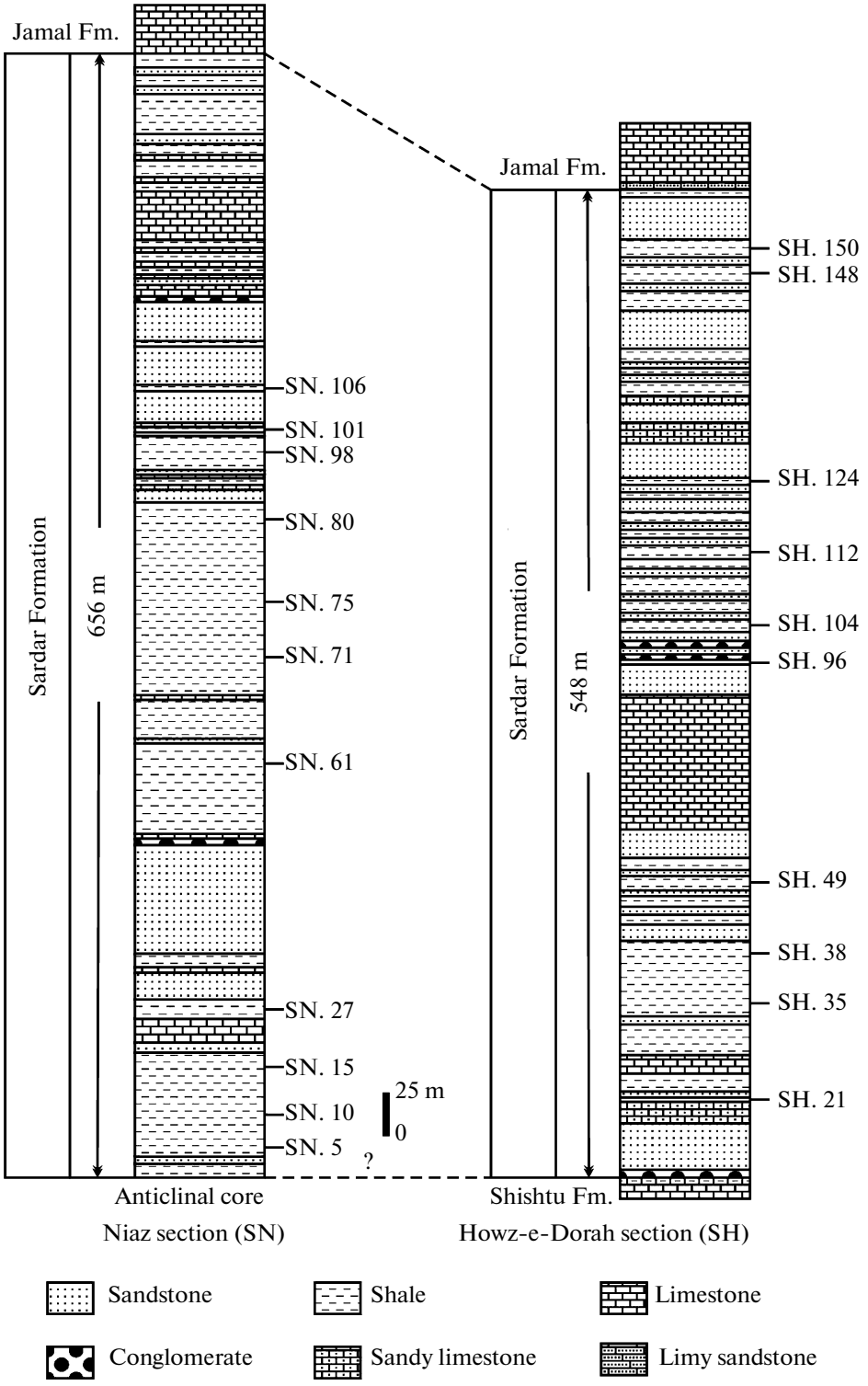

Fig.3. Columnar sections of the Sardar Formation, showing sample locations.

and their post depositional impermeability. However, the concentrations of element in shales are affected by sedimentary processes such as weathering in source area, transportation from source area to depositional basin. The element such as K, Na, Mg and Ca concentrations are enriched or depleted by these environmental processes, while another element such as Zr, Ti and Al are unaffected by these processes due to low solubility of their oxides and hydroxides in low temperature aqueous solutions [15, 27, 28].

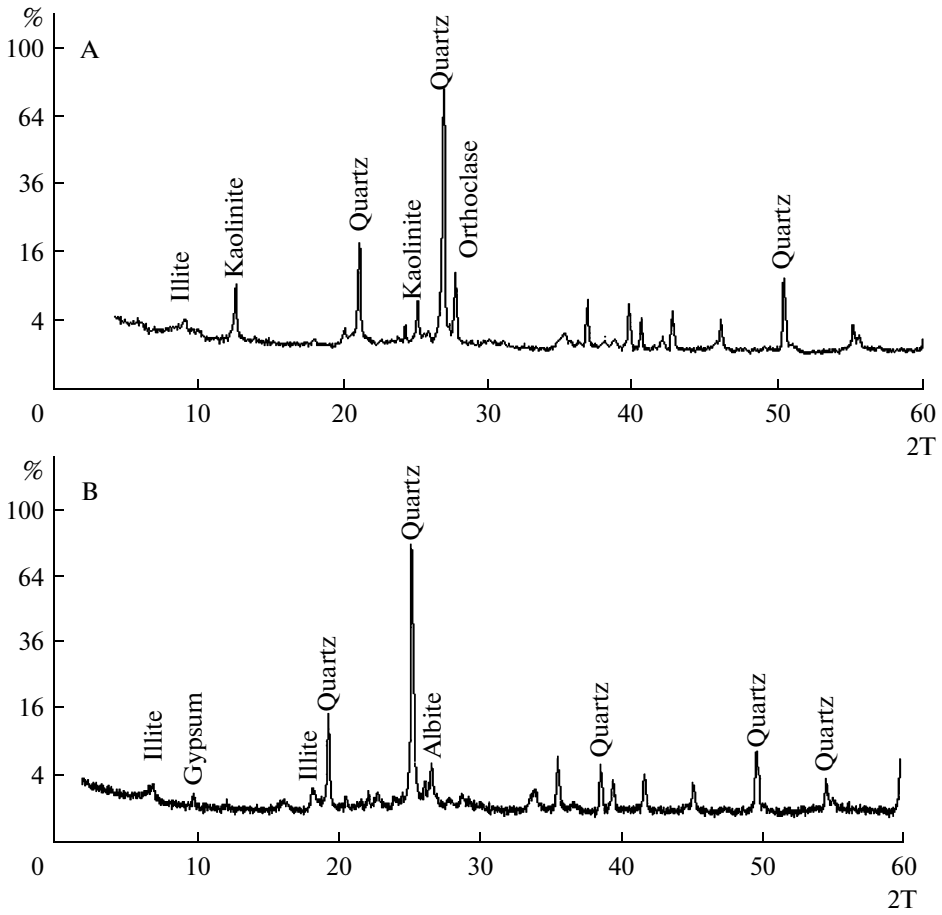

Fig. 4. A: X-ray diffraction pattern of sample SH.96, B: X-ray diffraction pattern of sample SN. 106.

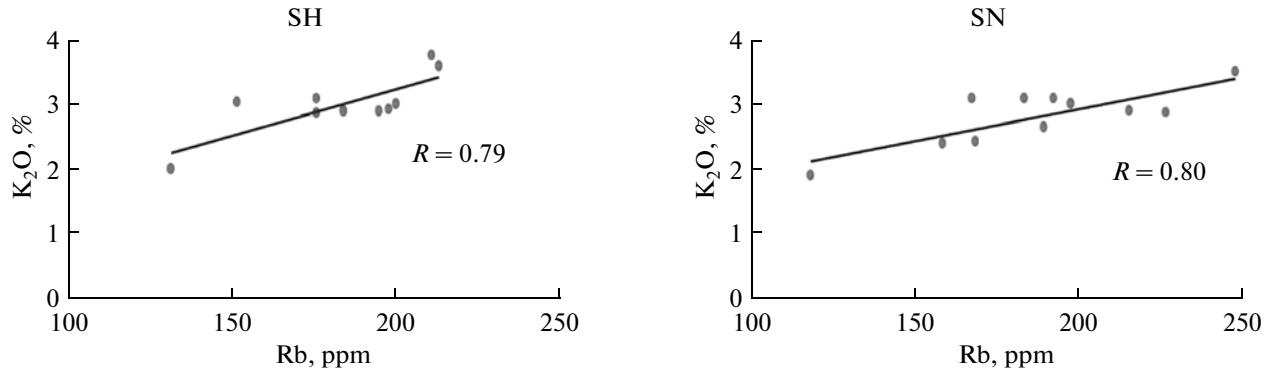

Fig. 5. Positive linear correlation coefficients between K_2O and Rb (SN: Niaz section and SH: Howz-e-Dorah section).

The major and trace element analyses of the shales of Sardar formation collected from the two stratigraphic sections are listed in Table 1 and 2. Many elements have clear positive linear correlation coefficients with K_2O such as Th and Rb (Fig. 5) that shows the absolute abundances of these elements are primarily controlled by illite. The plot Al_2O_3, versus TiO_2 is used commonly for determining source rock compositions [11, 29]. A positive correlation is evident between Al_2O_3 and TiO_2 in shales. The plot Al_2O_3 versus TiO_2 for Niaz and Howz-e-Dorah sections concentrate near the granodiorite-granitic field (Fig. 6). Concentration of Zr is used for analysis compositional of source rocks [15]. Zr content of the Niaz shales varies from 667 to 1236 ppm and for Howz-e-Dorah shales is from 520 to 1073 ppm that is similar to the average value for granite.

Table 1. Major element (oxide % wt) concentrations of shales

Sample No.	SiO_2	Al_2O_3	Na_2O	MgO	K_2O	TiO_2	MnO	CaO	P_2O_5	Fe_2O_3	SO_3	LOI
SN.5	69.08	16.76	1.01	0.82	2.66	0.78	0.00	0.53	0.06	3.89	0.00	3.92
SN.10	71.88	14.20	1.01	0.97	1.92	0.70	0.01	0.56	0.05	4.84	0.00	3.42
SN.15	68.37	16.26	0.84	0.66	3.12	0.75	0.00	0.48	0.06	4.97	0.00	3.95
SN.27	69.58	17.99	0.93	0.52	3.02	0.82	0.00	0.31	0.08	2.10	0.08	3.90
SN.61	68.86	15.80	1.17	0.98	2.45	0.77	0.04	0.57	0.07	5.55	0.01	3.28
SN.71	69.32	17.21	1.11	0.83	2.88	0.86	0.00	0.48	0.05	3.17	0.00	3.67
SN.75	70.84	15.99	1.12	0.80	2.42	0.83	0.00	0.55	0.05	3.53	0.00	3.41
SN.80	67.96	17.01	0.99	1.01	2.91	0.80	0.01	0.43	0.05	4.29	0.00	4.08
SN.98	68.24	18.90	0.77	0.61	3.53	0.94	0.00	0.24	0.04	1.60	0.06	4.56
SN.101	70.68	14.77	1.06	0.86	3.10	0.87	0.02	0.11	0.04	2.44	0.67	4.86
SN.106	66.46	16.09	0.76	0.87	3.12	0.80	0.01	0.42	0.05	1.41	3.51	5.93
SH.21	50.69	22.76	0.10	0.82	3.02	1.03	0.04	1.69	0.14	9.34	0.04	9.75
SH.35	67.37	20.00	0.19	0.42	2.03	0.79	0.00	0.41	0.08	1.65	0.29	6.20
SH.38	64.67	19.97	0.10	0.42	2.90	0.87	0.00	0.32	0.06	2.38	1.05	6.69
SH.49	59.17	25.48	0.29	0.60	2.91	1.16	0.00	0.25	0.17	1.58	0.13	7.61
SH.96	71.03	17.47	0.02	0.44	3.11	0.74	0.00	0.26	0.08	2.20	0.00	4.19
SH.104	62.98	20.31	0.02	0.69	3.61	0.97	0.02	0.71	0.10	3.69	0.00	6.40
SH.112	65.85	19.44	0.06	0.58	3.78	0.95	0.01	0.83	0.07	2.37	0.00	5.54
SH.124	64.75	21.96	0.03	0.60	2.92	1.00	0.01	0.24	0.07	2.23	0.00	5.53
SH.148	67.19	17.66	0.05	0.55	3.06	0.85	0.01	0.43	0.05	3.94	0.00	5.75
SH.150	52.99	26.59	0.13	0.67	2.95	1.21	0.01	0.11	0.07	3.75	0.34	10.59

Note: LOI = Loss of ignition, SH = Howz-e-Dorah and SN = Niaz sections.

The plot of Zr versus TiO_2 can be used to differentiate three different source rocks, such as, felsic, intermediate and mafic igneous rocks. The Zr versus TiO_2 plot of the Sardar Formation shales represents predominantly felsic-intermediate igneous source rocks (Fig. 7). The TiO_2/Zr weight ratio generally increases with decreasing SiO_2 content, from >200 for mafic igneous rocks, 55 to 195 for intermediate igneous rocks and <55 for felsic rocks [15]. The TiO_2/Zr weight ratio for all Sardar Formation shales is < 20 that represents predominantly felsic igneous source rocks. The average K_2O/Na_2O ratio of the Niaz samples vary from 1.9 to 4.58 and for Howz-e-Dorah is from 29 to 180.5. The average SiO_2/Al_2O_3 ratio of the Niaz shales vary from 3.61 to 5.06 and for Howz-e-Dorah samples is from 1.99 to 4.06. However, plot of K_2O/Na_2O versus SiO_2/Al_2O_3 for shales of Sar-

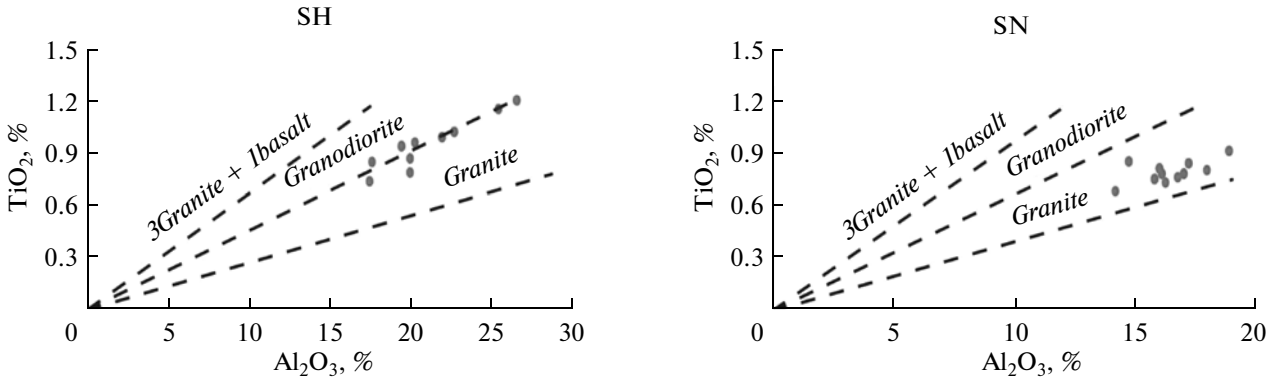

Fig. 6. The plot Al_2O_3 versus TiO_2 for the Niaz and Howz-e-Dorah shales. The granite line and 3 granite + 1 basalt line are from [11] (SN: Niaz section and SH: Howz-c-Dorah section).

Table 2. Trace element (ppm) concentrations of shales

Sample No.	Rb	Sr	V	Zr	Zn	Sc	La	Ba	Co	Cr	Cu	Nb	Ni	U	Th
SN.5	190	248	167	767	166	3	64	361	20	107	65	32	25	8	12
SN.10	119	209	148	808	137	4	60	286	42	88	65	23	61	1	10
SN.15	193	219	155	786	305	4	60	332	29	92	57	23	107	21	21
SN.27	198	802	144	908	49	3	47	317	12	87	40	23	15	1	18
SN.61	169	260	158	715	139	5	58	587	35	112	39	19	39	2	23
SN.71	227	206	158	667	110	3	63	329	17	123	59	29	52	13	18
SN.75	159	227	161	783	115	2	70	355	34	79	60	22	19	7	13
SN.80	216	210	165	696	155	3	46	394	35	116	51	25	45	15	22
SN.98	248	245	165	900	54	2	41	370	18	103	55	32	N	9	20
SN.101	184	173	150	1083	81	2	47	297	22	89	51	26	13	8	17
SN.106	168	239	155	1236	89	2	53	262	28	66	42	25	40	6	15
SH.21	199	485	378	520	209	9	43	408	83	253	64	33	121	12	24
SH.35	131	586	208	834	40	2	61	286	13	131	46	22	13	6	18
SH.38	175	393	210	978	30	3	45	364	11	143	33	24	N	12	11
SH.49	183	579	294	1019	57	3	63	376	21	153	56	44	59	11	30
SH.96	175	348	148	718	46	3	35	416	30	101	79	18	39	14	15
SH.104	212	422	208	645	86	4	70	387	22	126	66	36	34	5	16
SH.112	210	394	185	694	89	3	41	439	22	103	61	32	46	7	23
SH.124	194	489	210	1073	41	3	50	345	16	134	69	43	35	10	22
SH.148	151	257	195	642	169	4	39	385	31	119	63	33	44	13	23
SH.150	197	584	315	653	78	5	53	357	38	204	71	61	78	19	23

Note: N = not detected, SH = Howz-e-Dorah and SN = Niaz sections.

dar Formation show that most of shales plot in the field representing phanerozoic shale composition (Fig. 8). This shows that clay minerals in these shales control the major element composition which is diluted by increasing SiO_2 content [19, 31].

The ternary K_2O–Fe_2O_3–Al_2O_3 (Fig. 9) diagrams show that all shales of Sardar Formation are plotted near Al_2O_3 apex that is indicating enrichment of Al_2O_3 and also suggests that clay minerals control the element abundance [30].

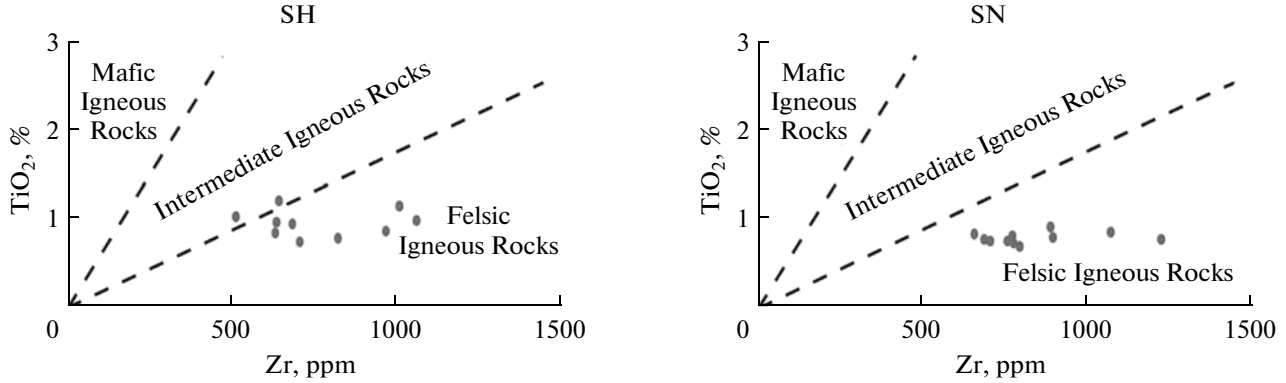

Fig. 7. Zr versus TiO_2 plot for the shales of Sardar Formation (after [15]) (SN: Niaz section and SH: Howz-e-Dorah section).

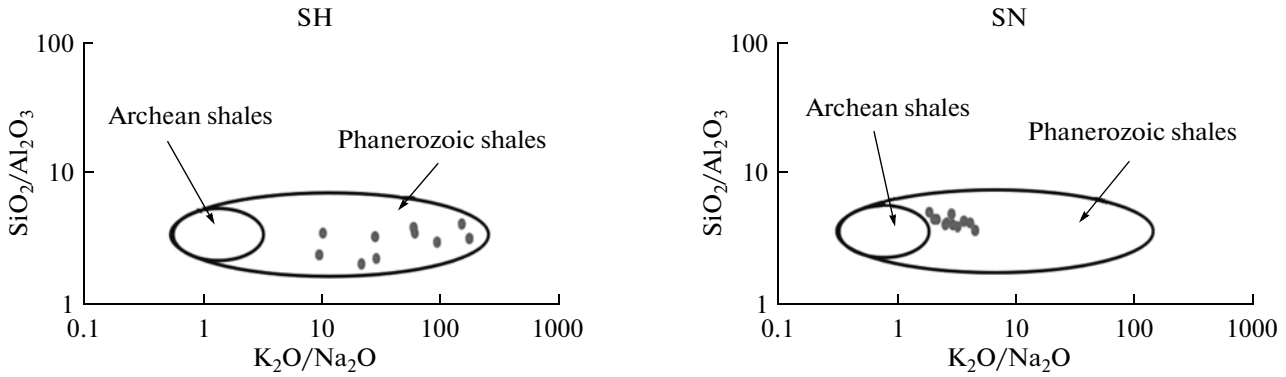

Fig. 8. Plot K_2O/Na_2O versus SiO_2/Al_2O_3 for shales of Sardar Formation. Fields for the Archean Greenstone shales and Phanerozoic shales from [30]. (SN: Niaz section and SH: Howz-e-Dorah section).

The K_2O/Al_2O_3 ratio of sediments can be used as an indicator of the original composition of ancient sediments. The K_2O/Al_2O_3 ratio for feldspars and clay minerals are different and varies from 0.3 to 0.9 and 0.0 to 0.3, respectively [33]. K_2O/Al_2O_3 ratio for Shales of Niaz and Howz-e-Dorah succession is 0.13 to 0.21 and 0.1 to 0.19, respectively. In all samples, K_2O/Al_2O_3 ratios are close in field of clay minerals range that this show the illite is the dominant clay mineral in these shales. The ratio of Al_2O_3/TiO_2 in mudrocks is similar to parent rocks [15]. The ratio of Al_2O_3/TiO_2 of shales are usually used to infer the source rock compositions, due to this ratio increases from 3 to 8 for mafic igneous rocks, from 8 to 21 for-intermediated igneous rocks and from 21 to 70 for felsic igneous rocks [15], The ratio of Al_2O_3/TiO_2 for Niaz and Howz-e-Dorah sections are ranges 16.97 to 21.93 and 20.46 to 25.31, respectively. Al_2O_3/TiO_2 ratio of these shales suggests that these sediments may have been derived from intermediated to felsic igneous rocks. The ratios of Th/Sc, Th/Co, Th/Cr and La/Sc are indicators for felsic and mafic rocks [30, 33, 35]. The ratios of Th/Sc, Th/Co, Th/Cr and La/Sc for these shales are compared with those of sediments derived from felsic and basic rocks as well as to upper continental crust and Post Archean Australian shales (PAAS) (Table 3) that show these ratios are in the field of felsic rocks. The La/Sc versus Th/Co plot suggests that these shales were drived from acidic rocks (Fig. 10).

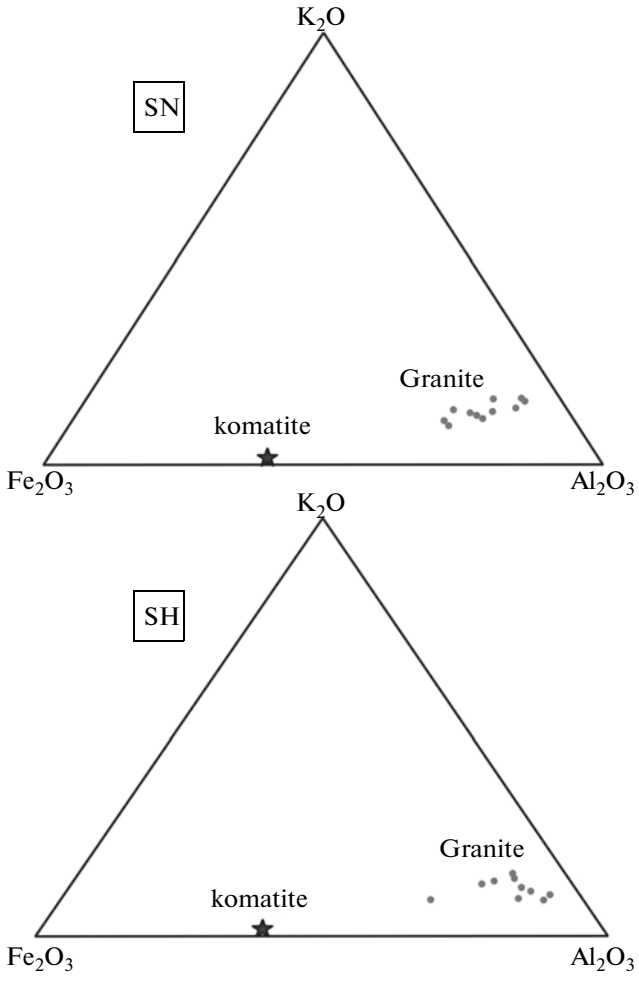

Fig. 9. Ternary K_2O–Fe_2O_3–Al_2O_3 diagram for shales of Sardar Formation (SN: Niaz section, SH: Howz-e-Dorah section) (diagram after [32]).

4.3. Tectonic Setting

Plot of SiO_2 versus K_2O/Na_2O is commonly used for identification of tectonic setting of shales that they were deposited in passive margins, active continental margins and oceanic island arc margins [10, 36]. In this binary diagram, all samples from both sections are plotted in passive margins field (Fig. 11). Therefore, based on this study, sediments derived from stable continental areas. [36] for sandstones and argillites of selected New Zealand terrancs used a discriminate function analysis elements (TiO_2, Al_2O_3, total Fe_2O_3, MgO, CaO, Na_2O and K_2O) in discriminating four different provenance groups including: 1—mafic, 2—intermediate-domi-

Table 3. Range of elemental ratios of shales of Sardar Formation in this study compared to the ratios in similar fraction derived from felsic, mafic rocks, upper continental crust and Post-Archean Australian shale

Elemental ratio	Range of shales from the Sardar Formation		Range of sediments [3, 52–54]		Upper continental crust	Post-Archean Australian shale [55]
	Niaz section	Howz-e- Dorah section	Felsic rocks	Mafic rocks		
Th/Sc	2.5–10	2.67–10	0.84–20.5	0.05–0.22	0.79	0.9
Th/Co	0.24–0.77	0.29–1.43	0.67–19.4	0.04–1.4	0.63	0.63
Th/Cr	0.11–0.23	0.08–0.22	0.13–2.7	0.018–0.046	0.13	0.13
Cr/Th	4.38–8.92	4.48–10.54	4.00–15	25–500	7.76	7.53
La/Sc	11.6–35	4.78–30.5	2.5–16.3	0.43–0.86	2.21	2.4

nantly andesitic detritus, 3—felsic and plutonic and volcanic detritus and 4—recycled mature polycyclic quartzose detritus. In this diagram (Fig. 12), all shales of Sardar Formation plotted in felsic and intermediate igneous rocks fields.

Sedimentary sorting and recycling can be monitored by a plot of Th/Sc versus Zr/Sc [7]. First-order sediments show a simple positive correlation between these ratios, while, recycled sediment show a substantial increase in Zr/Sc with far less increase in Th/Sc. On the Zr/Sc versus Th/Sc diagram (Fig. 13), all samples plotted in sediment recycling (zircon added). Also, the high concentration of Zr and Th relative to the PAAS in these shales could be due to the concentration of certain accessory mineral such as Zircon and monazite.

The results of our study can be correlated with paleomagnetic and paleotectonic maps of the Carboniferous period of the world [37]. The Iranian plate was probably positioned on the north-facing passive margin of Gondwana.

4.4. Paleoweathering and Paleoclimate in the Source Area

The chemistry of sedimentary rocks is controlled by the concentration in the composition of their source rocks, intensity of weathering processes, sedimentation conditions and diagenesis [38]. The weathering processes are governed mainly by tectonic and climate. The Chemical Index of Alteration (CIA) gives an indication of the degree of weathering in the source region [39]. The CIA index is calculated using the equation:

$$CIA = \{Al_2O_3/(Al_2O_3 + CaO + Na_2O + K_2O)\} \times 100.$$

Values are expressed as molar proportions and CaO represents CaO presents in silicate minerals only. The CIA value of nearly 100 is for kaolinite and chlorite, and 70–75 for average shale's [39]. CIA values for fresh granite is around 50 [40]. High values indicate intensive chemical weathering in the source area while low rates (i.e., 50 or less) indicate unweathered source areas. CIA values for the Sardar Formation shales vary from 77 to 80, with an average 79.5 for Niaz Section and from 80 to 89, with an average 85.14 for Howz-e-Dorah section that indicating the Sardar Formation shales were

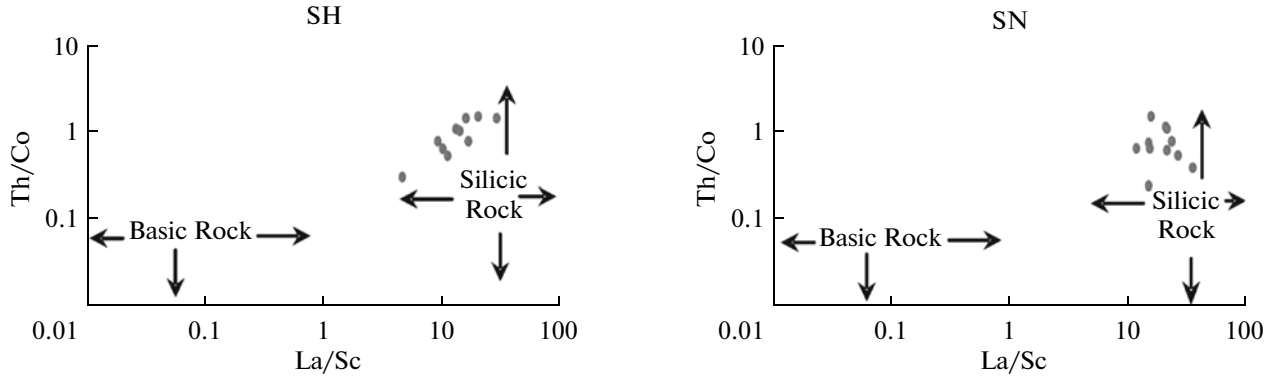

Fig. 10. La/Sc versus Th/Co plot for shales Sardar Formation (fields after [35]). (SN: Niaz section and SH: Howz-e-Dorah section).

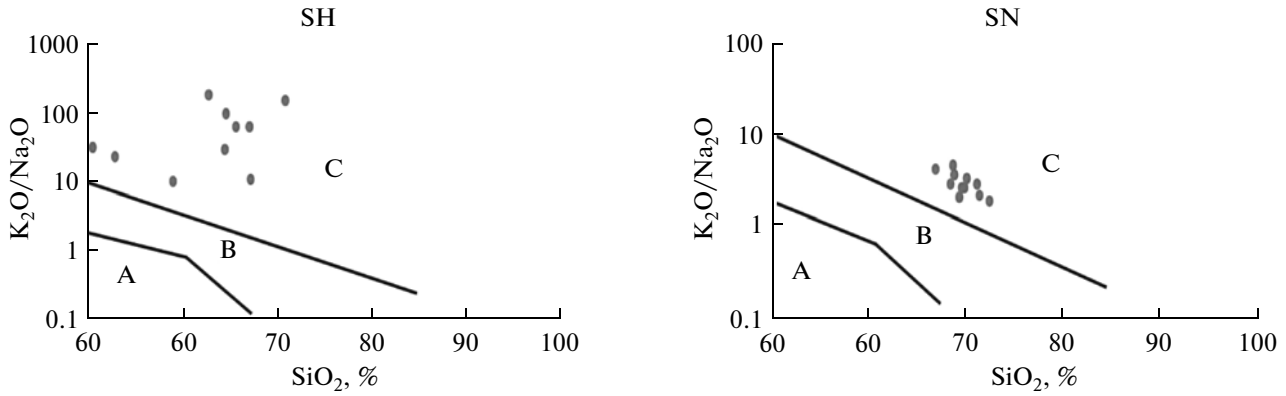

Fig. 11. Plot SiO_2 versus K_2O/Na_2O for shales of Sardar Formation (fields are demarcated after [10]). (SN: Niaz section and SH: Howz-e-Dorah section)
(A: Oceanic island margin, B: Active continental margin, C: Passive margin intracratonic).

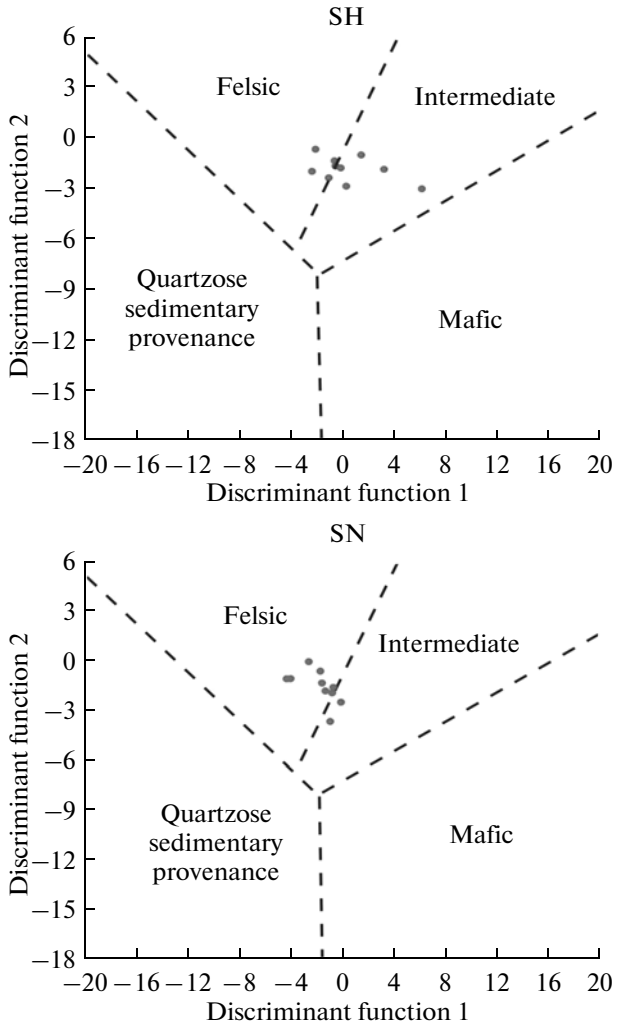

Fig. 12. Discriminant function diagram (after [36]) for shales of Sardar Formation, (SN: Niaz section and SH: Howz-e-Dorah section) Discriminant Function I: $-1.733TiO_2+0.607Al_2O_3+ 0.76Fe_2O_{3(t)}-1.5MgO+ 0.616CaO+0.509Na_2O-1.224K_2O-9.09$ Discriminant Function 2: $0.445TiO_2+0.07Al_2O3-0.25Fe_2O_{3(t)}- 1.142MgO+0.438CaO+1.475Na_2O+1.426K_2O-6.861$.

derived from high chemical weathering and indicate conversion of feldspar to clay minerals in the source areas during transport before deposition.

Post depositional diagenetic history and weathering of shales can be evaluated by plotting the CIA value in A-CN-K compositional ternary diagrams. In this ternary diagram (A: Al_2O_3, CN: CaO+ Na_2O and K: K_2O) [8, 9 and 41–43]. During initial stages of weathering the trend are parallel to the A–CN line due to destruction of plagiociasc feldspars and removal of Na and Ca at elements at this stage [6]. As weathering continues, k–feldspar is destroyed, releasing K and shifting the residual composition toward Al_2O_3. However, all samples plot near the Al_2O_3–K_2O joint (Fig. 14) that is indicating high to severe weathering condition in the source area.

In addition, paleoclimate and chemical maturity of fine grain terrigenous material delivered to the basin can also be deduced from chemical composition of the fine fraction of shales and metapelites [44, 45]. The Al_2O_3/TiO_2 ratio (<20 in humid conditions and >30 in arid climatic conditions) can be used as a climatic indicator for the source area. The average Al_2O_3/TiO_2 ratio of shales at Niaz and Howz-e-Dorah successions are 20.33 and 22.2, respectively, that indicates humid to semi humid-climate for the provenance area.

The index of compositional variability (ICV) can be measured, using the following formula [33]:

$$Fe_2O_{3(t)} + K_2O + Na_2O + CaO + MgO + TiO_2/Al_2O_3.$$

Where $Fe_2O_{3(t)}$ = total iron and CaO includes all source of Ca. In this index, the weight percents of the oxides are used rather than moles, and the values decrease with increasing degree of weathering. The ICV index indicates the degree of maturity of fine aluminosilicatic materials delivered to deposition basin [33]. ICV > 1 shows immature shales with a high percentage of silicate minerals (without clay minerals), while, more mature clayey rocks with abundant clay minerals proper have lower ICV values. The average

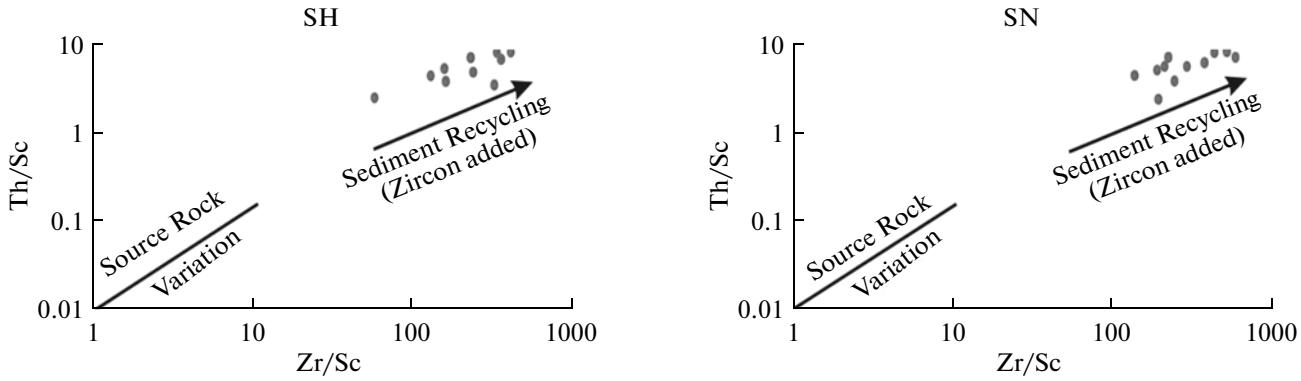

Fig. 13. The Zr/Sc and Th/Sc ratio increase going from mafic to felsic source area, but passive margin shales show anomalous Zr related to recycling of order sediments (after [7]). (SN: Niaz section and SH: Howz-e-Dorah section).

ICV for shales in the Sardar Formation at the Niaz and Howz-e-Dorah successions is 0.57 and 0.40, respectively, that shows all these shales are more mature clayey type rocks associated with abundant clay minerals such as Kaolinite and illites. Average basalt and average granite [46] yield strongly contrasting ICV values of 2.2 and 0.95. An interesting view of major element chemistry comes from a cross plot of CIA versus ICV values. Figure 15 shows that shales with this degree of weathering commonly derived from felsic and intermediated source rocks.

A robust agreement of palaeomagnetic poles of Iran and West Gondwana is observed for the Carboniferous, indicating that Iran was part of Gondwana during this time [48], During Carboniferous, an Iranian plate was located at 30°S (tropical climate). In this paleo-tropical succession, humid to semi-humid climate prevailed during the deposition of these shales.

4.5. Paleo-oxygenation Condition

Geochemical data have been used by various authors to understand the paleo-oxygenation condition of ancient sediments. The V/Cr ratio has been used as an index of paleo-oxidation in many studies [49, 50]. Ratios above 2 indicate anoxic conditions, while values below 2 suggest more oxidizing conditions [51]. The average V/Cr ratio for shales of Niaz section and Howz-e-Dorah section is 1.67 and 1.61, respectively (Table 4) that show these shales were deposited in oxic conditions. The Cu/Zn ratio is also used as a redox parameter [56]. While low Cu/Zn ratio indicates oxidizing conditions and high Cu/Zn ratio suggest reducing depositional conditions. However, the average Cu/Zn ratios for the shales of Niaz and Howz-c-Dorah successions are range from 0.51 and 0,97, respectively, that indicate all shales were deposited in oxidizing depositional conditions. The Ni/Co ratios below 5 indicate oxidizing environments, whereas ratio above 5 suggests suboxic and anoxic environments [51]. The Ni/Co ratio for shales of Niaz and Howz-e-Dorah sections are from

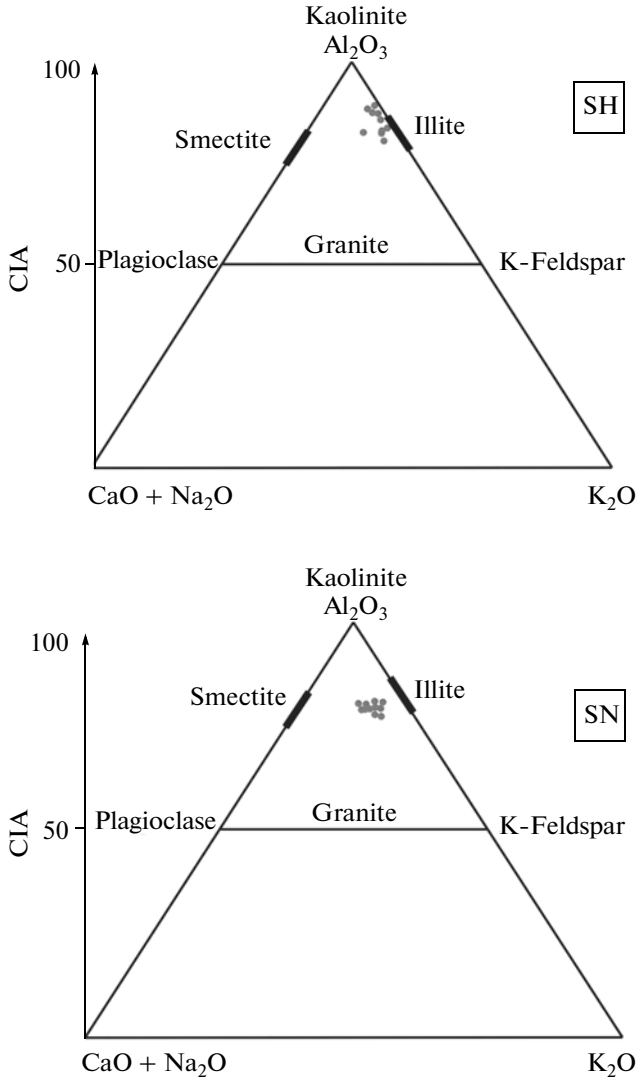

Fig. 14. A–CN–K ternary diagram for shales of Sardar Formation (SH: Howz-e-Dorah section, SN: Niaz section).

Table 4. Cu/Zn, Ni/Co and V/Cr as an index of paleo-oxidation for shales of Sardar Formation

Sardar Formation	V/Cr	Ni/Co	Cu/Zn
Niaz section	1.41–2.34 Average: 1.67	0.56–3.68 Average: 1.49	0.19–1.01 Average: 0.51
Howz-e-Dorah section	1.47–1.92 Average: 1.61	1–2.81 Average: 1.71	0.31–1.72 Average: 0.97

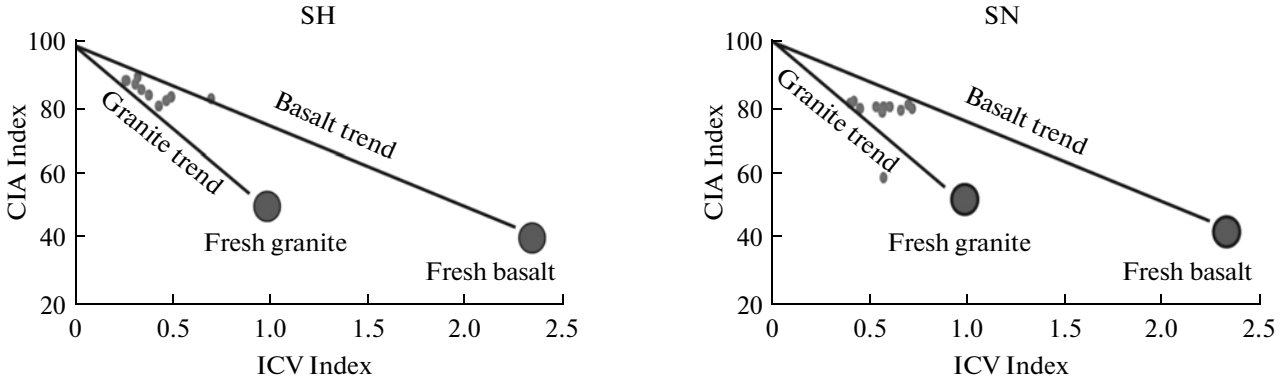

Fig. 15. Two indicators of weathering, Chemical index of Alteration (CIA) and Index of Chemical Variation (ICV) in shales of Sardar Formation (data of [47]).
(SN: Niaz section and SH: Howz-e-Dorah section).

0.56 to 3.68 and 1 to 2.81, respectively which show that these shales were deposited in oxidizing environments (Table 4).

5. CONCLUSION

The shales of Sardar Formation are rich in quartz, feldspar and phyllosilicates such as illites and Kaolinite. The Sardar Formation averages of the elemental ratios fall within the felsic source rocks. The geochemistry of these shales suggests that they formed by high weathering of acidic rocks. Al_2O_3/TiO_2 ratios also suggest source rocks of granitic and intermediated igneous rocks.

The large SiO_2 contents and large K_2O/Na_2O ratios reflect derivation from stable cratonic area or passive margin or tectonic quiescence. The geochemical data such as Ni/Co, V/Cr and Cu/Zn ratios show that these shales were deposited in oxidizing conditions. ICV values of the shales of Sardar Formation are less than 1 that suggesting they are compositionally mature and were dominated by recycling. In A–CN–K ternary diagram, all shales of the Sardar Formation plot parallel along the A–K line that indicate intense chemical weathering in the source area.

ACKNOWLEDGMENT

The authors would like to acknowledge the Ferdowsi University of Mashhad, Iran, for fieldwork and other logistic support. We would also like to acknowledge the editor of Geochemistry International Journal (Prof. M. A. Levitan), and anonymous reviewers for their review and suggestions that improved our manuscript significantly.

REFERENCES

1. F. J. Pettijohn, *Sedimentary Rocks*, 3rd edition (Harper and Row, New York, 1975).
2. M. T. McCulloch and G. J. Wasserburg, "Sm–Nd and Rb–Sr Chronology of Continental Crust Formation," Science **200**, 1003–1011 (1978).
3. R. L. Cullers, "The Geochemistry of Shales, Siltstones, and Sandstones of Pennsylvanian–Permian Age, Colorado, U.S.A.: Implications for Provenance and Metamorphic Studies," Lithos **51**, 305–327 (2000).
4. P. Huntsman-Mapila, A. B. Kampunzu, B. Vink, and S. Ringrose, "Cryptic Indicators of Provenance from the Geochemistry of the Okavango Delta Sediments, Botswana," Sediment. Geol. **174**, 123–148 (2005).
5. A. M. Hessler and D. M. Lowe, "Weathering and Sediment Generation in the Archean: An Integrated Study of the Evolution of Siliciclastic Sedimentary Rocks of the 3.2 Ga Moodies Group, Barberton Greenstone Belt, South Africa," Precambrian Res. **151**, 185–210 (2006).
6. S. Paikaray, S. Banerjee, and S. Mukherji, "Geochemistry of Shales from the Paleoproterozoic to Neoproterozoic Vindhyan Supergroup: Implications on Provenance, Tectonic and Paleoweathering," J. Asian. Earth Sci. **32**, 34–48 (2008).
7. S. M. McLennan, S. R. Taylor, and K. A. Eriksson, "Geochemistry of Archean Shales from the Pilbara Supergroup, Western Australia," Geochim. Cosmochim. Acta **47**, 1211–1222 (1983).
8. H. W. Nesbitt and G. M. Young, "Prediction of Some Weathering Trends of Plutonic and Volcanic Rocks Based on Thermodynamic and Kinetic Consider-

ations," Geochim. Cosmochim. Acta **48**, 1523–1534 (1984).

9. H. W. Nesbitt and G. M. Young, "Formation and Diagenesis of Weathering Profiles," J. Geol. **97**, 129–147 (1989).
10. H. W. Nesbitt and G. M. Young, "Determination of Tectonic Settings of Sandstone–Mudstone Suites Using SiO_2 Content and K_2O/Na_2O Ratio," J. Geol. **94**, 635–650 (1986).
11. J. Schieber, "A Combined Petrographical–Geochemical Provenance Study of the Newland Formation, Mid-Proterozoic of Montana," Geol. Mag. **129**, 223–237 (1992).
12. H. W. Fedo, H. W. Nesbitt, and G. M. Young, "Unraveling the Effects of K-Metasomatism in Sedimentary Rocks and Paleosols, with Implications for Paleoweathering Conditions and Provenance," Geology **23**, 921–924 (1995).
13. C. M. Fedo, K. A. Eriksson, and E. J. Krogstad, "Geochemistry of Shales from the Archean (~3.0 Ga) Buhwa Greenstone Belt, Zimbabwe: Implications of Provenance and Source-Area Weathering," Geochim. Cosmochim. Acta **60**, 1751–1763 (1996).
14. C. M. Fedo, G. M. Young, and H. W. Nesbitt, "Palaeoclimatic Control on the Composition of the Paleoproterozoic Serpent Formation, Huronian Supergroup, Canada: a Greenhouse to Icehouse Transition," Precambrian Res. **86**, 201–223 (1997).
15. K. Hayashi, H. Fujisawa, H. D. Holland, and H. Ohmoto, "Geochemistry of ~1.9 Ga Sedimentary Rocks from Northeastern Labrador, Canada," Geochim. Cosmochim. Acta **61**, 4115–4137 (1997).
16. L. Zhang, M. M. Sun, S. Wang, and X. Yu, "The Composition of Shales from the Odos Basin, China: Effects of Source Weathering and Diagenesis," Sediment. Geol. **116**, 129–141 (1998).
17. M. D. Campo and S. R. Guevara, "Provenance Analysis and Tectonic Setting of Late Neoproterozoic Metasedimentary Succession in NW Argentina," J. Am. Earth Sci. **19**, 143–153 (2005).
18. F. Sugitani, T. Yamashita, K. Nagaoka, M. Yamamoto, K. Minami, Mimura and K. Suzuki, "Geochemistry and Sedimentary Petrology of Archean Clastic Sedimentary Rocks at Mt. Goldsworthy, Pilbara Craton, Western Australia: Evidence for the Early Evolution of Continental Crust and Hydrothermal Alteration," Precambrian Res. **147**, 124–147 (2006).
19. G. Deru, L. Xuexang, C. Pengehun, X. Bin. Guanghao, H. Bachinski, Zhuanli and F. Gonggu, "Mesoproterozoic–Neoproterozoic Transition: Geochemistry, Provenance and Tectonic Setting of Clastic Sedimentary Rocks on the SE Margin of the Yangtze Block, South China," J. Asian. Earth Sci. **29**, 637–650 (2007).
20. M. Alavi, "Tectonostratigraphic Synthesis and Structural Style of the Alborz Mountainous System in Northern Iran," J. Geodynam. **11**, 1–33 (1996).
21. A. M. C. Sengor, "The Cimmeride Orogenic System and the Tectonics of Eurasia," Geol. Soc. Am. Sp. Pap., no. 195 (1984).
22. *Atlas Tethys Paleoenvironmental Maps*, Ed. by J. Dercourt, L. E. Ricou, and V. Vrielynck (Cauthier–Villars, Paris, 1993).
23. C. R. Scotese and R. P. Langford, Langford, "Pangea and the Paleogeography of the Permian," in *The Permian of Northern Pangea*, Ed. by P. A. Scholle, T. M. Peryl, and D. S. Ulmer-Scholle (Spriger-Verlag, Berlin, 1995), Vol. 1, pp. 3–19.
24. G. Stampfli and A. Pillevuit, "An Alternative Permotriassic Reconstruction of the Kinematics of the Teyhan Realm," in *Atlas Tethys Paleoenvironmental Maps*, Ed. by J. Dercourt, L. E. Ricou, and V. Vrielynck (Cauthier–Villars, Paris, 1993), pp. 55–62.
25. Y. Lasemi, Facies Analysis, "Depositional Environments and Sequence Stratigraphy of the Upper PreCambrian and Paleozoic Rocks of Iran," Geol. Surv. Iran, (2001) [in Persian].
26. K. Lasemi, M. Ghomashi, H. Amin-Rasouli, and A. Kheradmand, "The Lower Triassic Sorkh Shale Formation of the Tabas Block, East Central Iran: Succession of Failed-Rift at the Paleotethys Margin," Carbonate and Evaporites, **23** (1), 21–38 (2008).
27. W. Stumm and J. J. Morgan, Morgan *Aquatic Chemistry: An Prologue Emphasizing Chemical Equilibra in Natural Waters* (Wileys, New York, 1981).
28. K. Sugitani, Y. Horiuchi, and M. Adachi, "Anomalously Low Al_2O_3/TiO_2 Values for Archean Cherts from the Pilbara Block, Western Australia—Possible Evidence for Extensive Thermal Weathering on the Early Earth," Precambrian Res. **80**, 49–76 (1996).
29. S. M. McLennan, W. B. Nance, and S. R. Taylor, "Rare Earth Element Thorium Correlations in Sedimentary Rocks and the Composition of the Continental Crust," Geochim. Cosmochim. Acta **44**, 1833–1839 (1980).
30. D. J. Wronkiewicz and K. C. Condie, "Geochemistry of Archean Shales from the Witwatersrand Supergroup, South Africa: Source Area Weathering and Provenance," Geochim. Cosmochim. Acta **51**, 2401–2416 (1987).
31. A. B. Kampunzu, J. L. H. Cailteux, B. Moine, and H. N. B. T. Loris, "Geochemical Characterization, Provenance, Source and Depositional Environment of Roches Argilo-Talqueuses (TAR) and Mines Subgroups Sedimentary Rocks in the Neoproterozoic Katangan Belt (Congo): Lithostratigraphic Implications," J. Afr. Earth Sci. **42**, 119–133 (2005).
32. K. C. Condie, "Chemical Composition and Evolution of the Upper Continental Crust: Contrasting Results from Surface Samples and Shales," Chem. Geol. **104**, 1–37 (1993).
33. R. Cox, D. R. Lowe, and R. L. Cullers, "The Influence of Sediment Recycling and Basement Composition on Evolution of Mudrock Chemistry in the Southwestern United States," Geochim Cosmochim. Acta **59** (14), 2919–2940 (1995).
34. R. L. Cullers, "The Controls on the Major and Trace Element Evolution of Shales, Siltstones, and Sandstones of Ordovician to Tertiary Age in the Wet Mountain Region, Colorado, U.S.A," Chem. Geol. **123** (1–4), 107–131 (1995).
35. R. L. Cullers, "Implications of Elemental Concentrations for Provenance, Redox Conditions, and Metamorphic Studies of Shales and Limestones near Pueblo, CO, USA," Chem. Geol., **191** (4), 305–327 (2002).
36. B. P. Roser and R. J. Korsch, "Provenance Signatures of Sandstone–Mudstone Suites Determined Using

Discriminant Function Analysis of Major-Element Data," Chem. Geol. **67**, 119–139 (1988).

37. J. Golonka, "Phanerozoic Paleoenvironment and Paleolithofacies Maps, Late Paleozoic," Geologia **33**, 145–209 (2007).
38. P. K. Zawada, "The Stratigraphy and Sedimentology of the Ecca and Beaufort Group in the Fouresmith Area, South Western Orange Free State," Geol. Surv. S. Afr. **90**, (1988).
39. H. W. Nesbitt and G. M. Young, "Early Proterozoic Climates and Plate Motions Inferred from Major Element Chemistry of Lutites," Nature **299**, 715–717 (1982).
40. J. N. J. Visser and G. M. Young, "Major Element Geochemistry and Paleoclimatogy of the Permo–Carboniferous Glacigene Dwyka Formation and Post-Glacial Mudrocks in Southern Africa," Palaeogeogr. Palaeoclimatol. Palaeoecol. **81**, 49–57 (1990).
41. H. W. Nesbitt, C. M. Fedo, and G. M. Young, "Quartz and Feldspar Stability, Steady and Non-Steady-State Weathering and Pedogenesis of Siliciclastics Sands and Muds," J. Geol. **105**, 173–191 (1997).
42. G. M. Young and H. W. Nesbitt, "Paleoclimatology and Provenance of the Glaciogenic Gowganda Formation (Paleoproterozoic), Ontario, Canada: a Chemostratigraphic Approach," Geol. Soc. Am. Bull. **111**, 264–274 (1999).
43. H. W. Nesbitt, Petrogenesis of Siliciclastic Sediments and Sedimentary Rocks, in *Geochemistry of Sediments and Sedimentary Rocks*, Ed. by D. R. Lenz, Geotext 4, (Geol. Ass. Canada, New Foundland, 2003), pp. 39–51.
44. E. P. Akulshina, "Evolution of Physicochemical Conditions of Sedimentation in the Riphean and Phanerozoic (with Siberia as Example)," in *Environment and Life in Geological Past* (Nauka, Novosibirsk, 1990), pp. 17–26.
45. V. A. Melezhik, "Model of the Evolution of Precambrian Basins of Sedimentary Rock Formation on the Baltic Shield," Izv. Akad. Nauk SSSR, Ser. Geol., No. 5, 139–148 (1991).
46. Y. H. Li, *A Compendium of Geochemistry* (Princeton Univ., Princeton, 2000).
47. Y. I. Lee, "Provenance Derived from the Geochemistry of Late Paleozoic–Early Mesozoic Mudrocks of the Pyeongan Supergroup, Korea," Sediment. Geol. **149**, 219–235 (2002).
48. G. Muttoni, M. Mattei, M. Balini, A. Zanchi, M. Gaetani and F. Berra, "The Drift History of Iran from the Ordovician to the Triassic," Geol. Soc. London, Sp. Publ. **312**, 7–29 (2009).
49. H. Dill, "Metallogenesis of Early Paleozoic Graptolite Shales from the Graefenthal Horst (Northern Bavaria–Federal Republic of Germany)," Econ. Geol. **81**, 889–903 (1986).
50. H. Dill, M. Teshner, and H. Wehner, "Petrography, Inorganic and Organic Geochemistry of Lower Permian Carboniferous Fan Sequences (Brandschiefer Series) FRG: Constraints to their Palaeogeography and Assessment of their Source Rock Potential," Chem. Geol. **67** (3–4), 307–325 (1988).
51. B. Jones and D. C. Manning, "Comparison of Geochemical Indices Used for the Interpretation of Paleo-Redox Conditions in Ancient Mudstones," Chem. Geol. **111** (1–4), 111–129 (1994).
52. R. L. Cullers, "The Controls on the Major and Trace Element Variation of Shales, Siltstones and Sandstones of Pennsylvanian–Permian Age from Uplifted Continental Blocks in Colorado to Platform Sediment in Kansas, USA," Geochim. Cosmochim. Acta **58** (22), 4955–4972 (1994).
53. R. L. Cullers and V. N. Podkovyrov, "Geochemistry of the Mesoproterozoic Lakhanda Shales in Southeastern Yakutia, Russia: Implications for Mineralogical and Provenance Control, and Recycling," Precambrian Res. **104** (1–2), 77–93 (2000).
54. R. L. Cullers, A. Basu, and L. Suttner, "Geochemical Signature of Provenance in Sand-Size Material in Soils and Stream Sediments near the Tobacco Root Batholith, Montana, USA," Chem. Geol. **70** (4), 335–348 (1988).
55. S. R. Taylor and S. McLennan, *The Continental Crust: Its Composition and Evolution* (Blackwell, Oxford, 1985).
56. R. O. Hallberg, "A Geochemical Method for Investigation of Palaeoredox Conditions in Sediments," Ambio, Sp. Rept. **4**, 139–147 (1976).